Korean J. Chem. Eng., 40(4), 975-985 (2023)
DOI: 10.1007/s11814-022-1295-9

pISSN: 0256-1115
eISSN: 1975-7220

Mechanisms and kinetics of zinc and iron separation enhanced by calcified carbothermal reduction for electric arc furnace dust

Jiayong Qiu*,,****, Shui Yu*,***,****,†, Jiugang Shao***, Kaiqi Zhu*,****, Dianchun Ju*,****, Chunyu Chen*,****, Dexing Qi*,****, Fei Wang***, Ni Bai*,****, Rui Mao*,***,†, and Xiaoming Wang****

*School of Metallurgical and Materials Engineering, Jiangsu University of Science and Technology, Zhangjiagang 215600, China
**State Key Laboratory of Mineral Processing, Beijing 102628, China
***Institute of Research of Iron and Steel, Sha-Steel, Zhangjiagang 215625, China
****Institute of Fine Metallurgy Research, Industrial Technology Research Institute of Zhangjiagang & Jiangsu University of Science and Technology, Zhangjiagang 215600, China
(*Received 7 June 2022 • Revised 23 August 2022 • Accepted 15 September 2022*)

Abstract−A high basicity charge prepared with electric arc furnace dust (EAFD), carbonaceous reducing agent and CaO is proposed. The mechanisms of enhancing separation of zinc and iron by calcified carbothermic reduction of the high basicity charge were analyzed by combining thermal analysis kinetics and experiment. The influences of roasting temperature, carbon ratio (n_c/n_o, molar ratio of carbon in graphitic carbon powder to oxygen in EAFD), and CaO dosage on phase transition and dezincification ratio in EAFD were investigated. The results show that the intermediates $Ca_2Fe_2O_5$ and $Fe_{0.85-x}Zn_xO$ can be produced from the zinc-iron separation of zinc ferrate during the process of calcified carbothermic reduction of EAFD. Addition of CaO and C results in the following transition pathways: $ZnFe_2O_4$+CaO→$Ca_2Fe_2O_5$+ZnO→$Ca_2Fe_2O_5$+Zn(g)→CaO+Fe; $Fe_{0.85-x}Zn_xO$+CaO→$Ca_2Fe_2O_5$+FeO+ZnO→CaO+Fe+Zn(g). In the range of n_c/n_o of 0.4-1.2 and roasting temperature of 1,000-1,100 °C, the addition of CaO can promote reduction and dezincification. Based on the Kissinger-Akahira-Sunose (KAS) and Coats-Redfern methods, the kinetic results show that the calcified carbothermic reduction process can be divided into three stages: initial stage (α=0-0.3), middle stage (α=0.3-0.45), and final stage (α=0.45-1.0). The average activation energy of the initial stage is 305.01 kJ·mol^{-1}, and the reaction mechanism is one-dimensional diffusion. The average activation energy is 315.67 kJ·mol^{-1} for the middle stage and 288.22 kJ·mol^{-1} for the final stage. The chemical reaction equation is found to be the most suitable mechanism in the medium and final stages. It is also found that the addition of CaO can reduce the average activation energy by about 32 kJ·mol^{-1} and shorten the intermediate stage of the reaction.

Keywords: EAF Dust, Calcified Carbothermic Reduction, Phase Transition, Kinetics, Non-isothermal

INTRODUCTION

In 2021, electric arc furnace (EAF) steelmaking accounted for more than 28.9% of the world's total crude steel production [1]. Indeed, electric arc furnace dust (EAFD) is not only rich in iron, but also contains significant amounts of heavy metals such as zinc and lead, which is why it is often classified in the hazard class [2-5]. However, recovery and reuse of valuable elements such as Zn, Fe, and Pb in dusts can save energy and costs. In the disposal of dusts, valuable metals cannot be recovered either by direct landfilling or by stabilization/fixation processes. The former, in particular, can lead to the accumulation of heavy metals in groundwater and soil, which poses a threat to animals, plants, and the human environment [6]. Currently, the main technologies for EAFD treatment can be divided into pyrometallurgy and hydrometallurgy and their combined processes [7,8]. Unlike hydrometallurgical processes, pyrometallurgical processes with high dezincification ratio and high metallization degree have been extensively used in the Chinese steel industry for many years [9]. Therefore, the pyrometallurgical system is considered the preferred choice for EAFD recycling due to its high steel recovery, convenient residue disposal, and compact technology [10].

The main pyrometallurgical processes used to treat EAFD include carbothermal reduction [11], calcification [12], and halogenation [10,13]. The principle of carbothermal reduction is the reduction of metal oxides at high temperatures using carbonaceous materials as reducing agents. The Waelz kiln and the rotary hearth furnace (RHF) processes are widely used in the iron and steel industry because of their high dezincification ratio and metallization ratio. The Waelz kiln process is based on carbothermal reduction using coal to recover zinc and lead from EAFD with high zinc content at 1,200 °C [14,15]. The RHF process is used to process EAFD with lower zinc content at 1,300 °C [16]. Therefore, the recovery of EAFD in both processes requires high energy consumption. In the hope of minimizing the energy requirement of the Waelz kiln process, many researchers have investigated alternatives, such as solar thermal reduction [17]. Due to the excellent microwave coupling properties of

†To whom correspondence should be addressed.
E-mail: yushuijust@163.com, maorui0138@163.com

carbonaceous materials, researchers use carbothermal reduction to recover metallic zinc from sludge/dust by microwave energy [18].

Recently, calcification processes to recover zinc from EAFD by adding $CaCO_3$ or lime [19] have attracted increasing attention. Itoh proposed the process of lime addition and magnetic separation (LAMS) [20] to recover ZnO from EAFD and use solid slag as raw material for steel production. According to the LAMS process, the reagents $CaCO_3$, Fe_2O_3 and ZnO are thoroughly mixed in appropriate proportions and pressed into a 1.5 g tablet with a diameter of 10 mm, and then roasted at 1,173 or 1,373 K. In the reaction zone, highly stable zinc ferrite ($ZnFe_2O_4$) reacts with calcium oxide (CaO) to form zinc oxide (ZnO) and calcium ferrite ($Ca_2Fe_2O_5$). ZnO and $Ca_2Fe_2O_5$ can be separated due to their magnetic differences. In addition, Chairaksa-Fujimoto performed non-carbothermal pretreatment of EAFD by adding CaO, a process known as "CaO treatment" [19,21]. In the calcification process, $ZnFe_2O_4$ is completely converted to ZnO and $Ca_2Fe_2O_5$ at a lower temperature of 1,173 K and a molar ratio of calcium to iron (n_{Ca}/n_{Fe}) of 1.1 for one hour, and most halides and heavy metals volatilize preferentially at 1,373 K. During the calcification process, the $ZnFe_2O_4$ phase is reconstructed by adding CaO, i.e., $ZnFe_2O_4$ can completely react with CaO to form ZnO and $Ca_2Fe_2O_5$. Unlike the intractable $ZnFe_2O_4$, ZnO and $Ca_2Fe_2O_5$ can be effectively separated from the electric arc furnace dust by the next steps (e.g., magnetic separation [20], alkaline leaching [21], ammonia leaching [22]). Moreover, the added CaO can facilitate the separation of Zn and Fe in zinc-containing dust, which is due to the reduction of CO concentration in the atmosphere and the increase of dezincification ratio [12]. Therefore, in the reduction of zinc-containing dust, the addition of an appropriate amount of CaO can improve the separation of zinc and iron. In view of this, to improve the basic recovery of EAFD, a combination of calcification and carbothermal reduction roasting should be investigated. The addition of calcium oxide to reconstruct the mineral phase of zinc ferrite will produce calcium ferrite, which can reduce the consumption of carbon reducer in the process of carbothermal reduction while ensuring the dezincification ratio.

Therefore, a high basicity charge prepared with EAFD, carbonaceous reducing agent and CaO is suitable for reducing carbon and ensuring dezincification degree. The high basicity charge is expected to improve the separation and recovery of Zn and Fe from Zn-containing dust. The simultaneous treatment of calcification and carbothermal reduction can produce zinc oxide and semi-metallized burden at lower temperature and lower reducing agent. The dezincified semi-metallized charge can be returned to the blast furnace for reuse.

Consequently, the current research mainly focuses on the recovery technology and process of EAFD, while the mechanism of calcified carbothermal reduction reaction of zinc-bearing EAFD is not clear, which is extremely important for in-depth understanding and regulation of the reaction process. Therefore, the effects of temperature, carbon content and CaO dosage on the reaction of high basicity charge prepared with zinc-bearing EAFD, carbon and CaO were investigated. In this study, the phase transition, dezincification ratio and reaction kinetics of calcified carbothermal reduction roasting of EAFD were analyzed.

EXPERIMENT

1. Materials

Zinc-containing samples were collected from the electric furnace plant of Sha steel in Jiangsu province, China. The chemical composition of the EAFD is shown in Table 1.

Fig. 1 shows the XRD (Ulitima IV, Nippon Rigaku Co.) pattern of EAFD, in which Fe is mainly present as $ZnFe_2O_4$, Fe_3O_4, Fe_2O_3 and $Ca_{0.15}Fe_{2.85}O_4$, and Zn is mainly present as $ZnFe_2O_4$ and ZnO.

Fig. 2 shows the particle size analysis of EAFD. The particle size is mainly 0.1-2.63 μm and 2.63-8.36 μm, respectively.

2. Experimental Procedure

The experiments consisted of five parts: Mixing, briquetting, calcified carbothermal reduction, XRD analysis, dezincification ratio analysis, and non-isothermal kinetic analysis. The specific experi-

Table 1. Chemical composition of the EAFD (wt%)

TFe	Zn	CaO	C	SiO_2	MgO	MnO	K_2O	SO_3
74.62	12.96	3.11	2.86	2.01	1.18	1.35	0.75	0.63

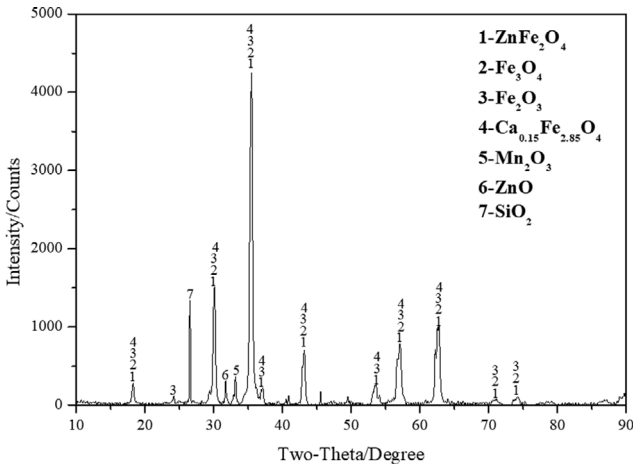

Fig. 1. XRD pattern of EAFD.

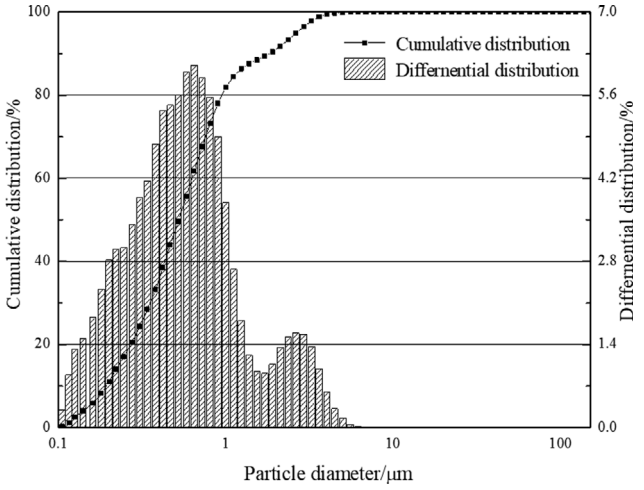

Fig. 2. Granular size composition of EAFD.

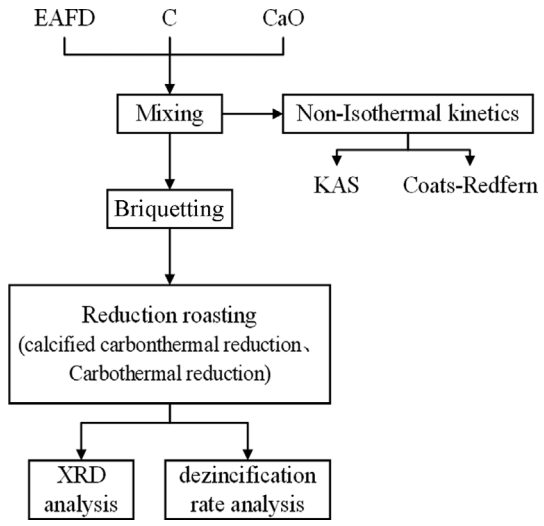

Fig. 3. Experiment and test flow chart.

mental procedure is shown in Fig. 3.

(1) Mixing. The dried EAFD, analytical pure reagent CaO and graphitic carbon powders were ground to the size of below 0.074 mm, respectively. Subsequently, EAFD and graphitic carbon were weighed and pre-blended according to various molar ratios of carbon in the graphitic carbon to oxygen in these EAFD reducible metal oxides (iron oxide and zinc oxide), i.e., n_c/n_o. After that, the pre-mixture of EAFD and graphitic carbon was remixed thoroughly with various amounts (3.21 wt%-7.16 wt%) of CaO and 0.6 wt% of carboxymethyl cellulose sodium (CMC, as a binder). The basicity (mass ratio of CaO to SiO_2 in the mixture) of the samples varied from 1.54 to 4.76.

(2) Briquetting. The mixtures of EAFD, graphite carbon, CaO and CMC powders were blended well by adding with 8 wt% of deionized water and compressed into a pellet at 20 MPa for 2 minutes. The tablets were dried at the temperature of 120 °C for 4 h.

(3) Reduction roasting. Each briquette was put into the alumina crucible, which was once then positioned in an atmosphere controlled high temperature tube furnace (Fig. 4). The sample was heated up to the set temperature and cooled with the furnace. The flow rate of the inlet N_2 used to be at 50 mL/min throughout the experiment.

(4) X-ray diffraction and dezincification ratio analysis. Each roasted briquette was cut along the center, crushed. A small amount of powder was taken to identify the mineralogical phase via X-ray diffraction analysis (XRD, Ulitima IV, Rigaku, Japan). The chemical composition of the roasted products used was decided with the aid of X-ray fluorescence spectroscopy (XRF, EDX-7000, Japan) and the dezincification ratio (η) was calculated according to Eq. (1):

$$\eta = \frac{m_0\omega_0 - m_1\omega_1}{m_0\omega_0} \times 100\% \quad (1)$$

where η - dezincification ratio; m_0 - initial mass of the sample, mg; m_1 - mass of the roasted product, mg; ω_0 - weight percentage of zinc in the initial sample; ω_1 - weight percentage of zinc in the roasted product.

(5) Non-isothermal kinetics analysis. The thermogravimetric experiments were carried out by a thermal gravimetric analyzer (TGA/DSC1), which consisted of a furnace body, a balance, an external water bath circulator and a computer. Each sample (30± 2 mg) was placed in the corundum crucible (Φ4.5 mm×5 mm) and then positioned in the thermogravimetric apparatus. Finally, the thermal gravimetric (TG) experiments were carried out beneath the atmosphere of N_2 with a flow rate of 20 mL/min at three different heating rates of 10, 20, and 30 °C/min. Based on the thermogravimetric data, the kinetics of the calcified carbothermal reduction of EAFD was analyzed by the non-isothermal method.

3. Theoretical Basis

This non-isothermal kinetic formula was expressed as follows:

$$\frac{d\alpha}{dt} = A\exp\left(-\frac{E_\alpha}{RT}\right)f(\alpha) \quad (2)$$

In the study, a heating rate β (°C/min) can be given as:

$$\beta = \frac{dT}{dt} \quad (3)$$

According to Eqs. (4) and (5), the non-isothermal kinetic formula should be:

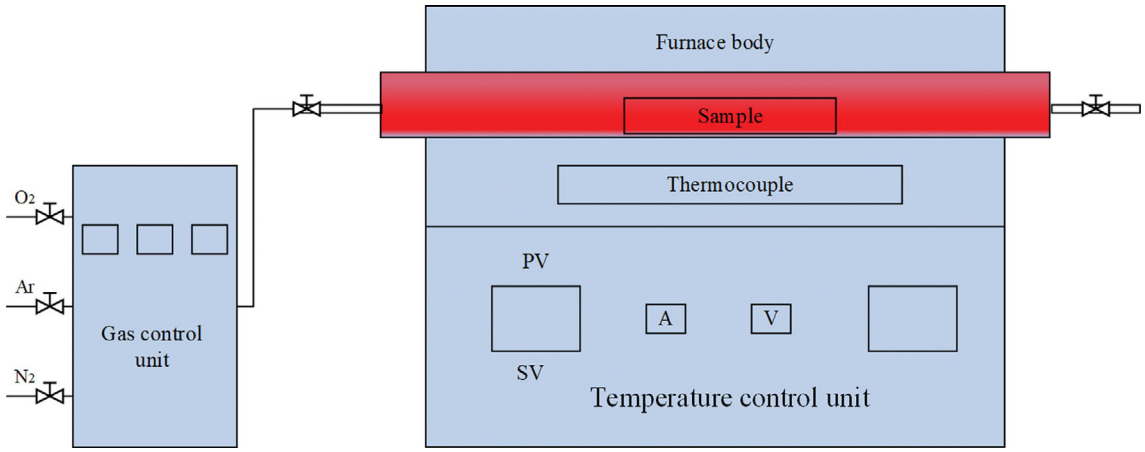

Fig. 4. Schematic diagram of atmosphere-controlled high-temperature tube furnace.

$$\frac{d\alpha}{f(\alpha)}=\frac{A}{\beta}\exp\left(-\frac{E_\alpha}{RT}\right)dT \quad (4)$$

where α is the conversion degree, T is thermodynamic temperature (K); β is heating rate (K·min^{-1}); E_α is activation energy (kJ·mol^{-1}); A is pre-exponential factor (s^{-1}); R is gas constant (8.314 J·mol^{-1}·K^{-1}); $f(\alpha)$ is model function.

3-1. Isoconversion Method (Kissinger-Akahira-Sunose Model)

The isoconversion method is widely applied because it can find the stable and reliable activation energies without involving the specific kinetic model functions. Among them, the reaction kinetics parameters were calculated by KAS method, according to the same conversion of TG curves at different heating rates [23-25]. The formula for KAS should be:

$$\ln\left(\frac{\beta}{T^2}\right)=\ln\left(\frac{AE_\alpha}{RG(\alpha)}\right)-\frac{E_\alpha}{RT} \quad (5)$$

From Eq. (5), E_α can be obtained from the linear representation of $\ln\beta/T^2$ versus 1/T for a given value of conversion, α.

3-2. Activation Energy Verification

To verify the activation energy obtained by using KAS method, the activation energy was calculated by Flynn-Wall-Ozawa (FWO) method [24,25]. The mathematical expression of FWO model is presented as follows:

$$\lg\beta=\ln\left(\frac{AE}{RG(\alpha)}\right)-2.315-0.4567\frac{E}{RT} \quad (6)$$

3-3. Coats-Redfern Methods

Coats and Redfern [26] proposed the model-fitting method for inferring the most probable kinetic model function. The equation is expressed as follows:

$$\ln\left(\frac{G(\alpha)}{T^2}\right)=\ln\left(\frac{AE}{\beta R}\right)-\frac{E}{RT} \quad (7)$$

where α is conversion rate; T is thermodynamic temperature (K); β is heating rate (K·min^{-1}); E is activation energy (kJ·mol^{-1}); A is preexponential factor (s^{-1}); R is gas constant (8.314 J·mol^{-1}·K^{-1}); $G(\alpha)$ is differential function.

The most probable mechanism model function can be inferred in phrases of the values of correlation coefficient (R-square) for the chosen 41 reaction model functions [27] by plotting the values of $\ln(G(\alpha)/T^2)$ versus 1/T and fitting with a method of least squares linear regression.

RESULTS AND DISCUSSION

1. Phase Transition Analysis

For illuminating the mechanism of zinc and iron separation enhanced by the addition of CaO during the carbothermal reduction of EAFD, the phase evolution of reduced samples under the conditions, including different temperatures, carbon ratios and calcium oxide additions, was analyzed by XRD, as shown in Figs. 5, 6 and 7.

The XRD patterns of the major minerals at different temperatures for 45 min with and without added CaO under n_c/n_o=0.8 are shown in Fig. 5. It can be seen that without adding CaO, the diffraction peak of carbon is clear and the intensity of the diffraction peak of $ZnFe_2O_4$ is weakened below 900 °C. When the temperature rises to 900 °C, the diffraction peaks of ZnO and Zn appear, indicating that the carbon thermal reduction of $ZnFe_2O_4$ occurs at this time. After adding CaO, $ZnFe_2O_4$ reacts with CaO to form $Ca_2Fe_2O_5$, which can be reduced to CaO and Fe with increasing temperature. At the calcination temperature of 1,000 °C, the carbon still has obvious diffraction peak compared with that without adding CaO. The residual carbon indicates that the consumption of reducing agent can be reduced by adding CaO. Meanwhile, the intensity of the diffraction peak corresponding to $ZnFe_2O_4$ decreases, indicating that the reduction of $ZnFe_2O_4$ can be enhanced by adding CaO. The diffraction peaks in the range of 41°-45° were

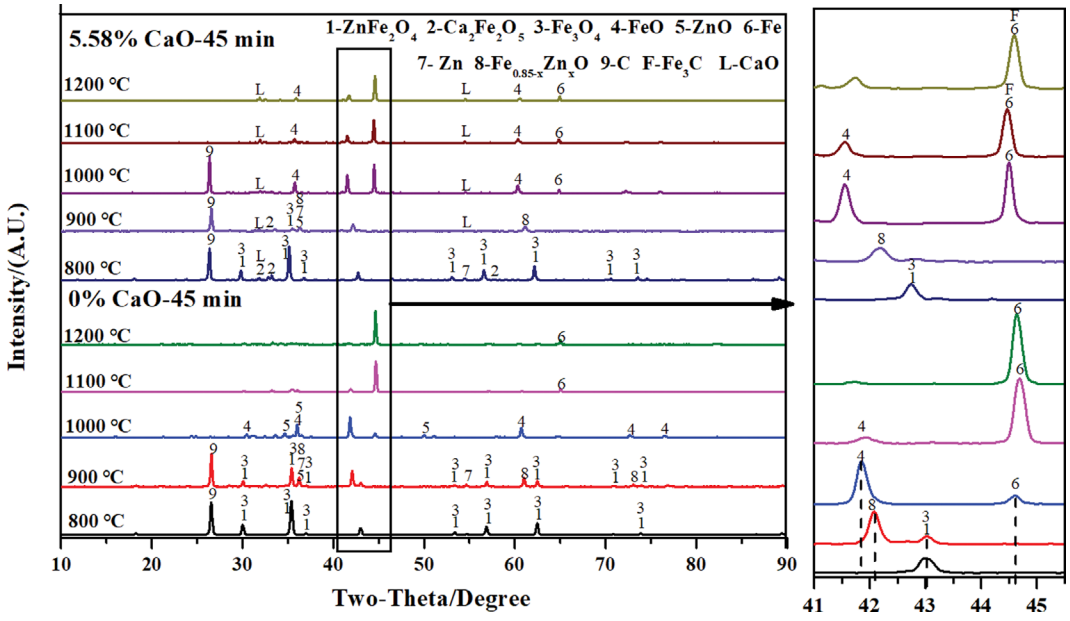

Fig. 5. XRD patterns of samples reduced at different temperatures for 45 min with and without adding CaO under n_c/n_o=0.8.

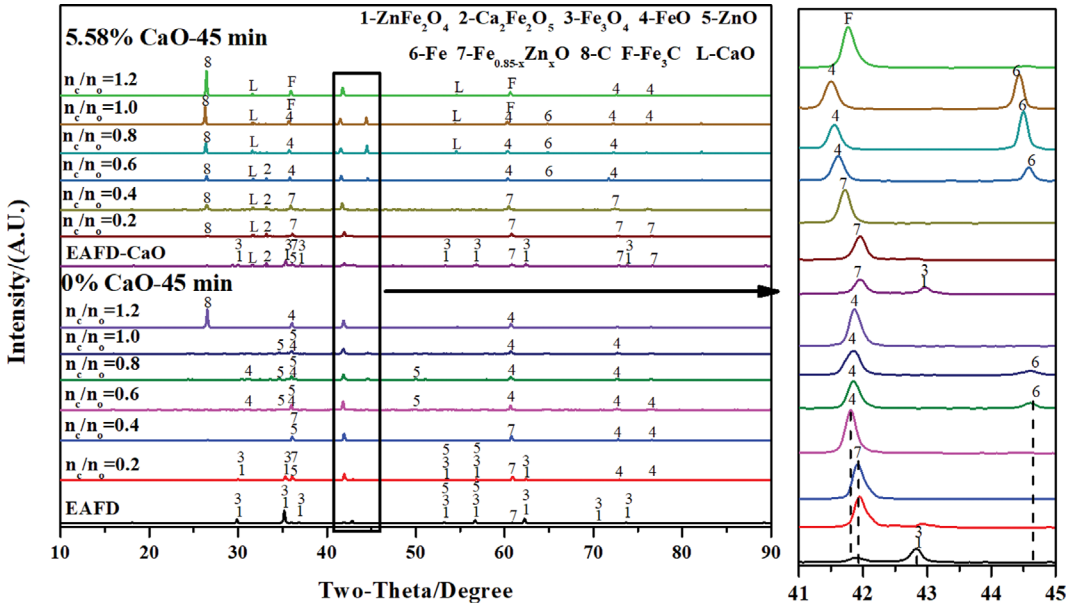

Fig. 6. XRD patterns of samples reduced at 1,000 °C for 45 min under different n_c/n_o with and without added CaO.

amplified. It is found that the Zn-Fe solid solution ($Fe_{0.85-X}Zn_xO$) is formed by carbothermic reduction of $ZnFe_2O_4$ at 900 °C regardless of the addition of CaO, which is considered to be one of the reasons affecting the separation of zinc and iron. Subsequently, with the increase of temperature, the diffraction peak of the zinc-iron solid solution shifts to the left and it is reduced to FeO or even Fe at 1,000 °C. At 1,100 °C, the diffraction peak of FeO is obviously weakened, while that of Fe is enhanced. It is also found that the diffraction peak of Fe at 1,000 °C after adding CaO is stronger than that without adding CaO.

As can be seen from Fig. 6, when CaO is not added, an obvious diffraction peak of carbon appears at n_c/n_o=1.2, indicating carbon excess at this time. However, with the addition of CaO, an obvious carbon diffraction peak appears when n_c/n_o is greater than 0.2, and the intensity of the diffraction peak of carbon increases with the increase of the carbon content. It is further tested that the addition of CaO can decrease the consumption of reducing agent in the process of carbothermic reduction of EAFD. The diffraction peak of $ZnFe_2O_4$ disappears and that of $Ca_2Fe_2O_5$ appears in the reduction products, indicating that $Ca_2Fe_2O_5$ is formed by the reaction of CaO and $ZnFe_2O_4$ in EAFD at n_c/n_o=0.2. However, when n_c/n_o=0.8, the diffraction peak of CaO appears and that of $Ca_2Fe_2O_5$ disappears, indicating that $Ca_2Fe_2O_5$ has been reduced and decomposed into CaO by carbon. The diffraction peak of ZnO disappears at n_c/n_o=0.2. As can be seen from the enlarged view of the diffraction peaks at 41°-45°, with the increase of n_c/n_o from 0 to 0.6, the diffraction peak of $Fe_{0.85-x}Zn_xO$ increases gradually and shifts left to FeO, regardless of whether calcium oxide is added. With the addition of CaO, the diffraction peak of Fe appears at n_c/n_o=0.6, and the intensity of the diffraction peak increases with the increase of carbon content. However, without adding CaO, the weak diffraction peak of Fe appears at n_c/n_o=0.8. It is indicated that the addition of CaO is conducive to the reduction of iron and the separation of zinc and iron.

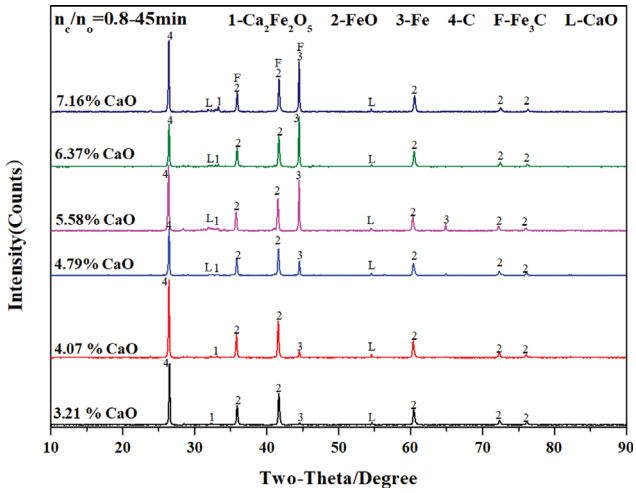

Fig. 7. XRD patterns of samples reduced at 1,000 °C for 45 min with different CaO dosages under n_c/n_o=0.8.

Fig.7 shows the XRD patterns of the samples reduced with different CaO dosages. It is shown that with the increase of CaO dosage from 3.21 wt% to 7.16 wt%, the phase composition of the reduced products does not change significantly, mainly composed of $Ca_2Fe_2O_5$, FeO, Fe, C and CaO. When CaO dosage is 7.16 wt%, the reduction product is carburized to form Fe_3C.

Fig. 8 presents the main phase transformation pathway in the calcified carbothermic reduction process of zinc-bearing EAFD based on these analyses. As the main phases of EAFD are $ZnFe_2O_4$ and Fe_3O_4, the main reaction pathway of its calcified carbothermic reduction is as follows:

$ZnFe_2O_4+CaO \rightarrow Ca_2Fe_2O_5+ZnO \rightarrow Ca_2Fe_2O_5+Zn(g) \rightarrow CaO+Fe$;
$Fe_{0.85-x}Zn_xO+CaO \rightarrow FeO+Ca_2Fe_2O_5+ZnO \rightarrow CaO+Fe+Zn(g)$;
$Fe_3O_4 \rightarrow FeO \rightarrow Fe$.

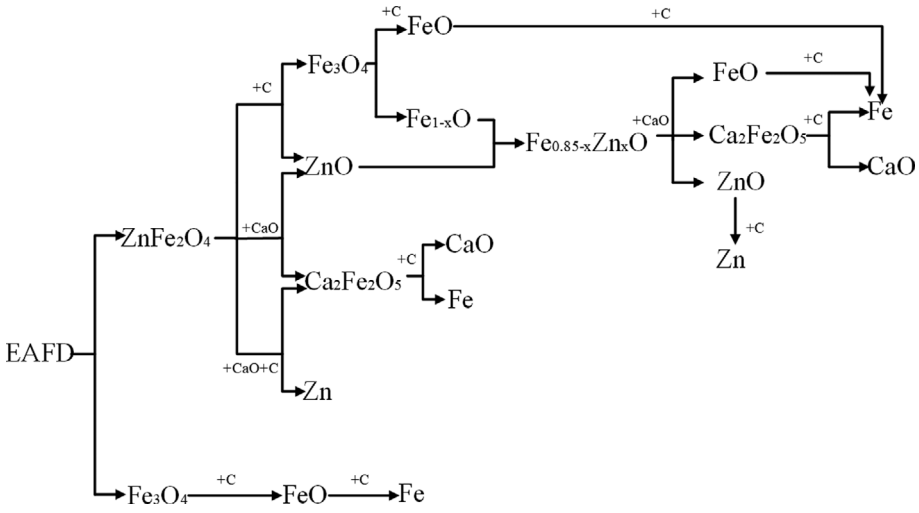

Fig. 8. Phase transition path of the carbothermal reduction of EAFD enhanced by CaO.

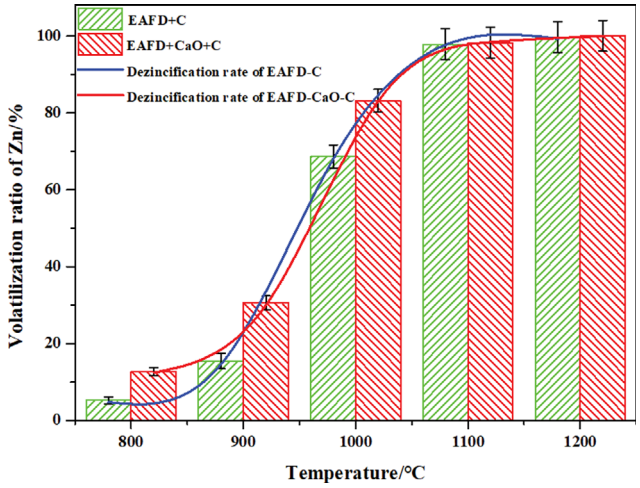

Fig. 9. The volatilization ratio of Zn at the different temperature.

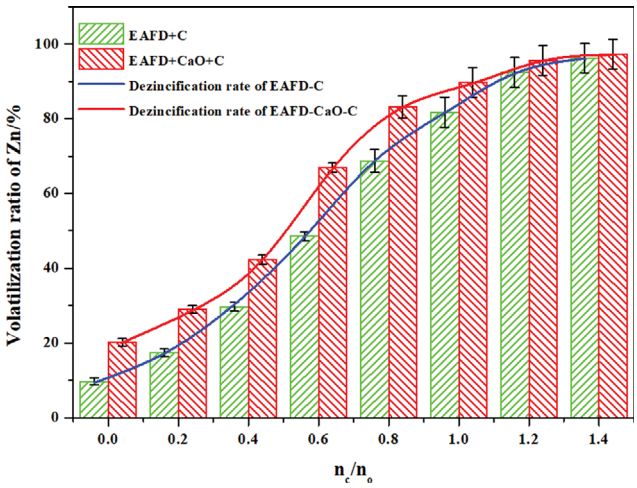

Fig. 10. The effect of n_c/n_o on the volatilization ratio of Zn.

2. Volatilization Ratio of Zn

The volatilization ratio of zinc at different temperature was analyzed under n_c/n_o=0.8, as illustrated in Fig. 9. In the range of 800-1,200 °C, increasing the roasting temperature is really useful to the volatilization of Zn and the addition of CaO significantly promotes the release of Zn. On the other hand, when the temperature is below 900 °C, the impact of CaO on the dezincification ratio is weak, and the zinc removal ratio is low whether CaO is added or not. With the increase of temperature from 900 °C to 1,000 °C, the volatilization of zinc increases significantly. This is due to the reaction of intermediate $Fe_{0.85-x}Zn_xO$ with CaO to form FeO, $Ca_2Fe_2O_5$ and ZnO, which promotes the separation of Zn and Fe. As from thermodynamic calculations by Iwase [28], it is clear that ZnO can be reduced to elemental zinc at 945 °C, and it has a boiling point of 907 °C, which causes the great expansion of zinc volatilization ratio. Therefore, when the temperature goes up to 1,000 °C, the promotion effect of CaO on zinc volatilization ratio is enhanced. However, above 1,100 °C, strong reduction conditions are favorable for the reduction of zinc oxide to Zn(g). It is indicated that CaO has no significant effect on improving dezincification ratio above 1,100 °C. In a word, for the sake of acquiring the significant contribution of CaO, the temperature should be between 1,000 °C and 1,100 °C.

The effect of carbon ratio on the zinc volatilization ratio in the carbothermal reduction of EAFD-C mixture and EAFD-CaO-C mixture was investigated under 1,000 °C for 45 min. The change of volatilization ratio of Zn is shown in Fig. 10. In the wake of carbon ratio, the zinc removal rate in both mixtures increases. However, at the same carbon ratio, the dezincification ratio of EAFD-CaO-C mixture is greater than that of EAFD-C. When CaO is added, the dezincification ratio is over 80% at n_c/n_o=0.8, which is slightly higher than that without CaO at n_c/n_o=1.0. When n_c/n_o is less than 0.4, the zinc volatilization ratio of EAFD-C mixture and EAFD-CaO-C mixture is lower than 50% and the intermediate product $Fe_{0.85-x}Zn_xO$ is obtained in the roasting process of both. At this time, the reducing conditions are poor, which is not conducive to the reduction of Zn-containing compounds, resulting in low zinc volatilization in the roasting process of both. When n_c/n_o is more than 1.2, there is little difference in the volatilization of zinc

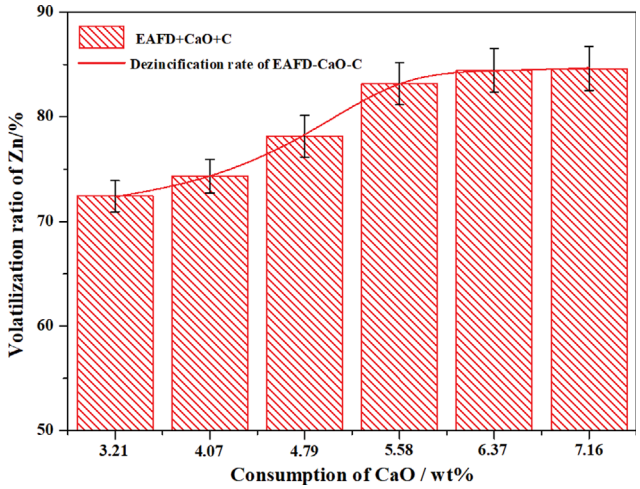

Fig. 11. The effect of consumption of CaO on the volatilization ratio of Zn.

between the samples with and without CaO due to better reduction conditions.

Fig. 11 shows the zinc volatilization ratio of reduction products with different consumption of CaO at the roasting temperature of 1,000 °C for 45 min. When the CaO dosage is lower than 5.58 wt%, the residual $ZnFe_2O_4$ in the EAFD that does not react with CaO needs to be reduced by carbothermal reduction to release zinc, which requires strong reducing conditions. The presence of trace SiO_2 and ZnO in the dust can lead to the slagging reaction, forming $2ZnO{\cdot}SiO_2$ which is difficult to reduce. When CaO is added, the slagging reaction between CaO and SiO_2 produces $2CaO{\cdot}SiO_2$, and the standard Gibbs free energy of the generated $2CaO{\cdot}SiO_2$ is less than that of the generated $2ZnO{\cdot}SiO_2$. Therefore, CaO can effectively inhibit the slagging reaction between SiO_2 and ZnO to improve the zinc volatilization. With the increase of CaO dosage from 5.58 wt% to 7.16 wt%, the effect of CaO on zinc volatilization is not significant. Therefore, taking economy and zinc volatilization into consideration, CaO dosage of 5.58 wt% is more effective.

3. Kinetic Analysis

3-1. Calcified Carbothermal Reduction Process of EAFD

Fig. 12 shows the TG and DTG (differential thermogravimetric) curves at heating rate of 10, 20, and 30 °C/min. The weight loss corresponding to the final temperature at different heating rates is essentially the same, but the mass loss at the lower heating rate is greater than that at the greater heating rate at the same temperature in the weight loss stage. This is because the lower the heating rate, the longer the residence time of the sample at each reaction temperature, i.e., the longer the reaction time at each temperature, the more complete the reaction. As shown in Fig. 12(b), there are two peaks on the DTG curves. As can be viewed that the first tiny peak appears in the temperature range of 800 °C to 900 °C and the second large peak in the range of 1,000 °C to 1,100 °C. It is shown that the rapid reaction corresponding to the large peak is consistent with the high zinc volatilization ratio at this temperature range, as described in Section 3.2. The transient decrease after the first tiny peak should indicate that the reaction is constrained by the solid solution ($Fe_{0.85-x}Zn_xO$) formed at 900 °C. With the increase of heating rate, the peak value of DTG curve increases and the starting and ending temperatures of the reaction increase. This is because the increase of heating rate shortens the total reaction time and strengthens the heat transfer hysteresis.

3-2. Conversion Degree Analysis

With the TG curves from Fig. 12, the degree of conversion (α) formula is expressed as follows:

$$\alpha = \frac{W_0 - W_t}{W_0 - W_\infty} \tag{8}$$

where W_0 and W_∞ (mg) are the initial and final weight of the sample, W_t is the weight of the sample at time t.

The conversion degree (α) under different heating rates is shown in Fig. 13. It is evident that the change trend of conversion degree curve is the same. With the increase of temperature, the conversion degree increases gradually and then flattens out. Fig. 14 shows the reduction rate ($d\alpha/dt$) versus conversion degree (α) at different heating rates. It is obvious that the reduction rate changes spectac-

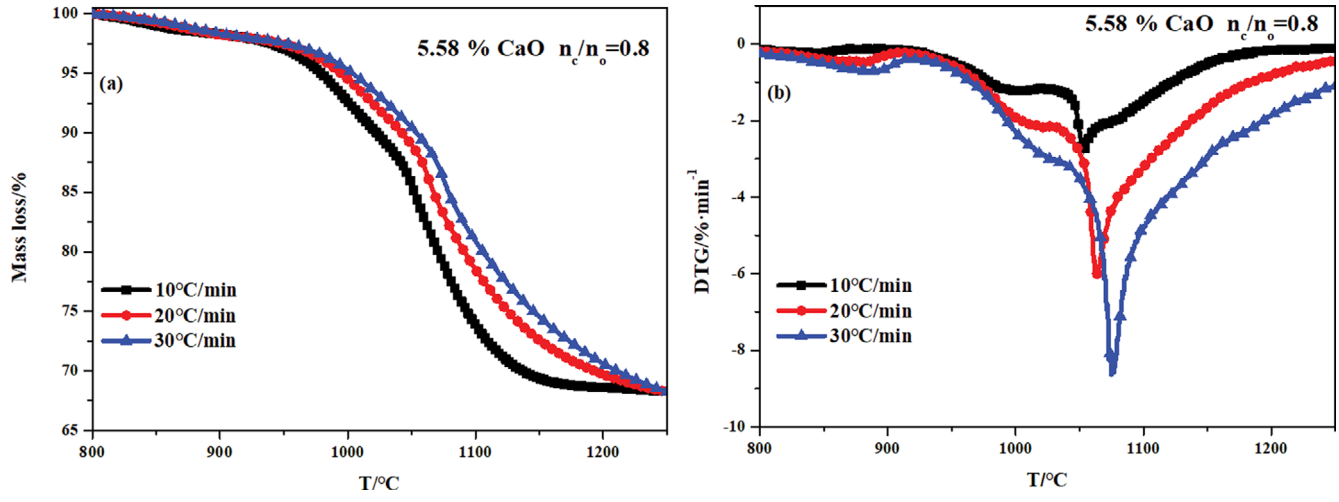

Fig. 12. TG (a) and DTG (b) curves of calcified carbothermal reduction of EAFD.

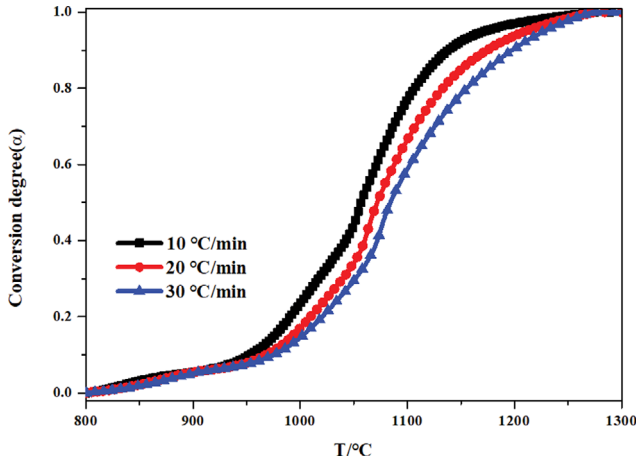

Fig. 13. Effect of heating rates on conversion degree of EAFD-CaO-C mixture.

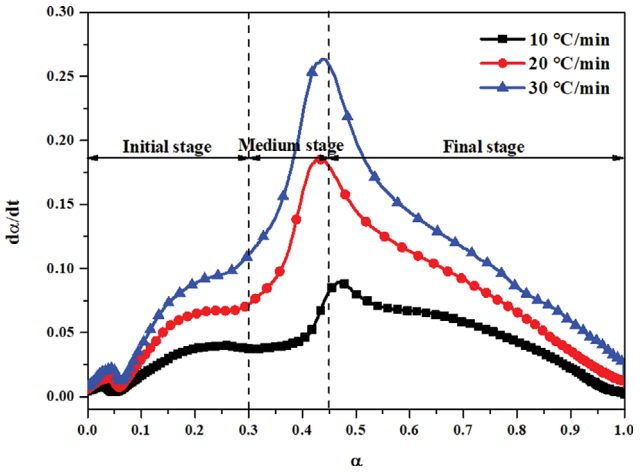

Fig. 14. Reaction rate (dα/dt) versus conversion degree (α) at different heating rates.

ularly all through the calcified carbothermal reduction of EAFD. The reduction rate increases gradually and then decreases as increasing in temperature. According to the results of activation energy and reaction rate curves, the reduction process of EAFD can be classified as three stages: α=0-0.3, α=0.3-0.45, and α=0.45-1.0.

3-3. Activation Energy Analysis

As shown in Fig. 15, the slopes of fitted lines can be used to determine the apparent activation energy values at different conversion degrees. Table 2 and Fig. 16 show the activation energy values with and without CaO acquired by the KAS method, the FWO method was used to verify the activation energy. As shown in Fig. 16, the activation energy curve is clearly divided into three sections by two turning points. The activation energy decreases from 373.09 to 261.92 kJ·mol^{-1} in the initial stage (α=0-0.3). The activation energy increases from 261.92 to 381.68 kJ·mol^{-1} within the

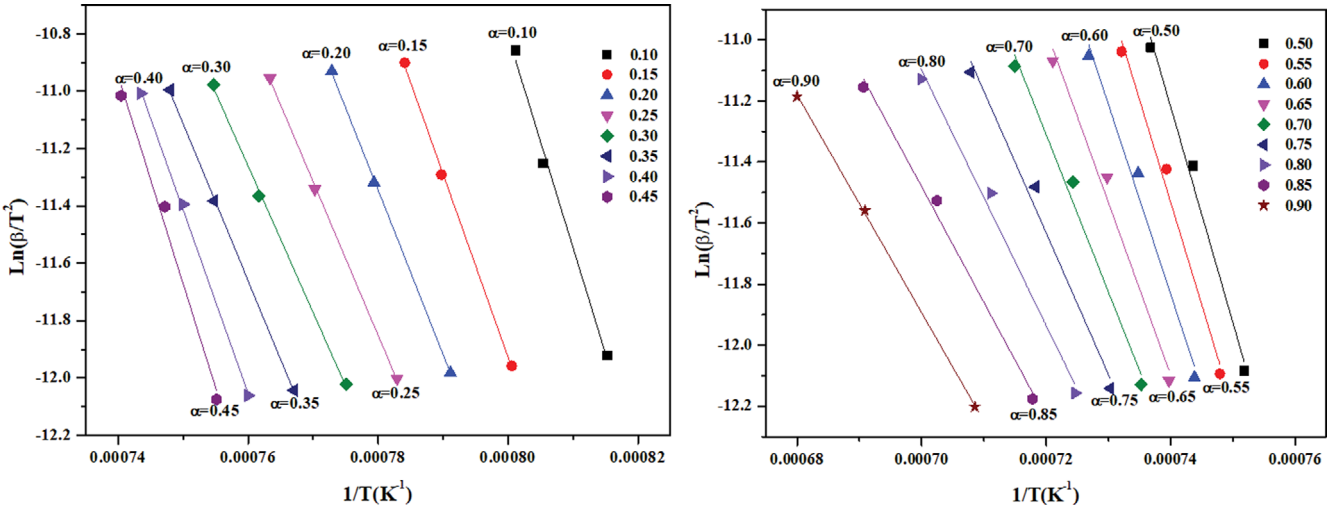

Fig. 15. Isoconversion nonlinear plots based on KAS method.

Table 2. Average activation energy of each reaction stage (kJ·mol^{-1})

		Initial stage	Medium stage	Final stage	Average
	α	0-0.3	0.3-0.45	0.45-1.0	
CaO addition	KAS	305.01	315.67	288.22	302.97
	FWO	300.21	316.79	292.10	303.03
	α	0-0.3	0.3-0.65	0.65-1.0	
Without CaO addition	KAS	310.96	354.94	337.00	334.30
	FWO	312.00	350.15	340.25	334.13

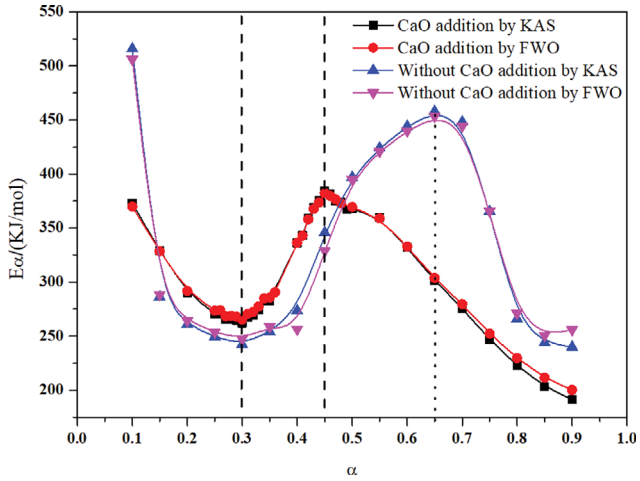

Fig. 16. Activation energies obtained by KAS and FWO methods.

conversion degree range of 0.3-0.45 (intermediate stage). When the reaction reaches α=0.45, the reaction enters the final stage (α=0.45-1.0), the activation energy starts to decrease gradually. The average activation energy values for the three stages are 305.01, 315.67 and 288.22 kJ·mol^{-1}, respectively. The average activation energy value of the whole reaction process is 302.97 kJ·mol^{-1}.

Obviously, Fig. 16 and Table 2 show the activation energy acquired with the aid of the KAS method is consistent with that by using the FWO method. The average activation energy of each stage with the addition of CaO is lower than that without CaO. The addition of CaO has a more significant effect on the medium and final stages. When CaO is not added, the range of medium stage is α= 0.3-0.65, while the medium stage is shortened by adding CaO.

3-4. Mechanism Mode Analysis

The Coast-Redfern method [26] was employed to decide the most probable mechanism model according to the model-fitting method shown in Fig. 17. The results of reaction kinetic are divided into three different stages: initial stage (α=0-0.3), intermediate stage (α=0.3-0.45) and final stage (α=0.45-1.0). At initial stage, the parabola rule is considered as mechanism model, which the equation $G(\alpha)=\alpha^2$ corresponds to one-dimensional diffusion. With regard to the medium stage, the reaction order n=4 is determined to be mechanism model, the chemical reaction model ($G(\alpha)=1-(1-\alpha)^4$) is considered as the kinetic model function. For the final stage, third-order reaction is determined as the mechanism model, where the chemical reaction has the dominant mechanism, its integral form

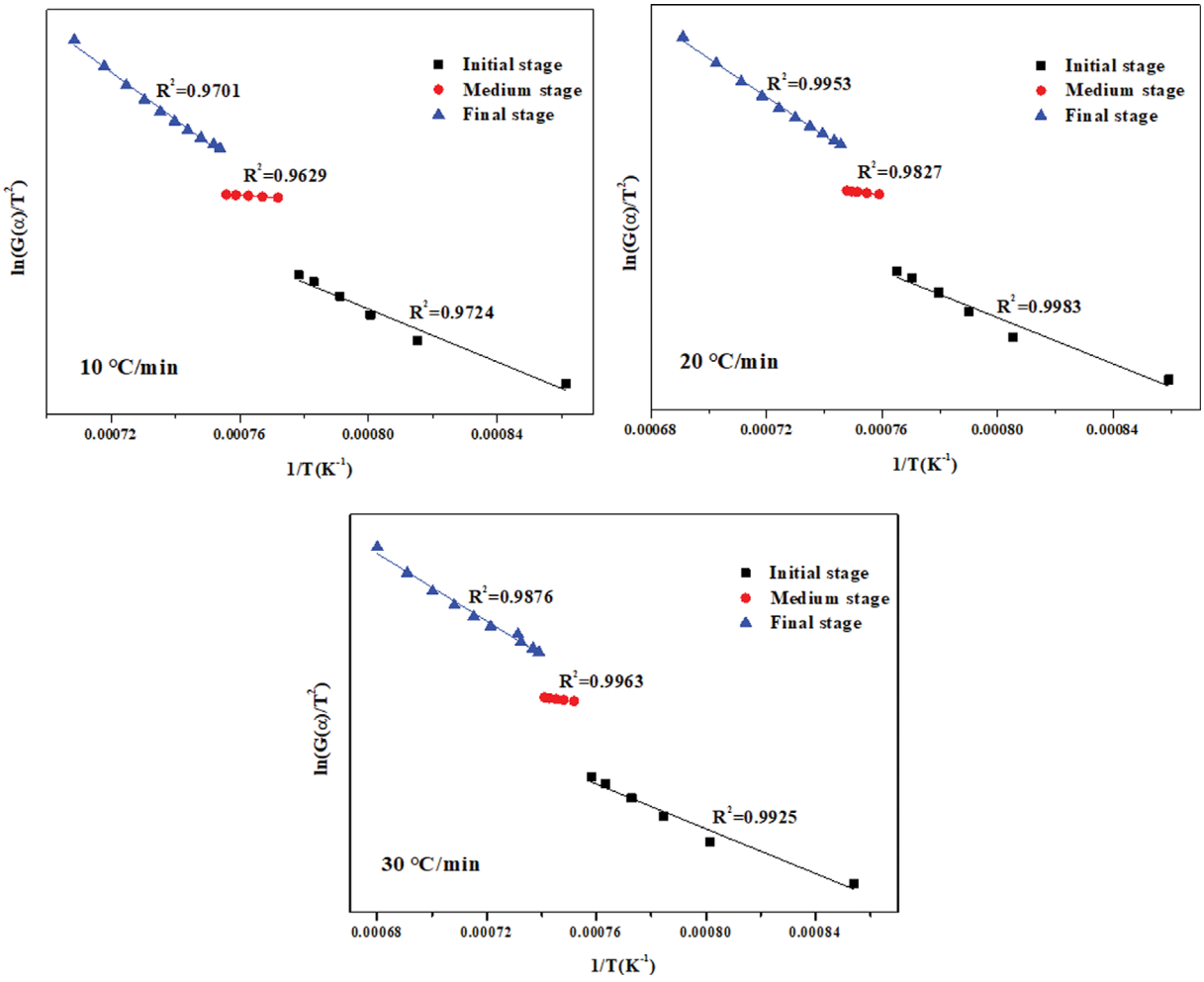

Fig. 17. Model-fitting plots of calcified carbothermal reduction process under different heating rates.

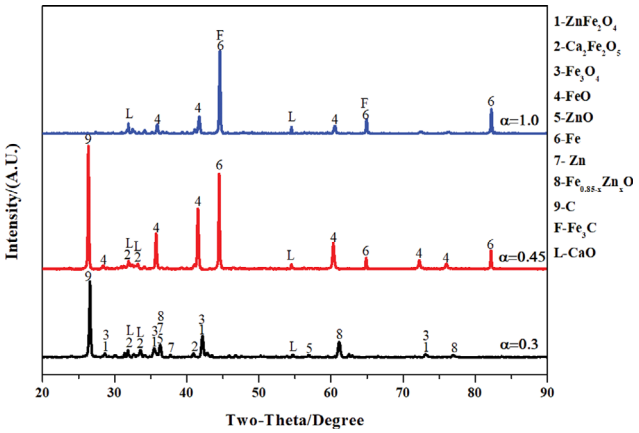

Fig. 18. XRD patterns of the products with conversion degrees (α) of 0.3, 0.45 and 1.0.

is $G(\alpha)=(1-\alpha)^{-2}$.

4. Enhanced Reduction Mechanism Analysis

Fig. 18 shows the XRD patterns of the products with conversion degrees (α) of 0.3, 0.45 and 1.0. It is indicated that the main phases include $ZnFe_2O_4$, $Ca_2Fe_2O_5$, Fe_3O_4, Zn, ZnO, $Fe_{0.85-x}Zn_xO$, CaO and C when the conversion degree is 0.3. As described in section 3.2, the reduction of ZnO to Zn can occur at α=0.3. The original phase of Fe_2O_3 has already been reduced, and its diffraction peaks are invisible. As a result, the main reactions that occur in the initial stage are shown as follows.

$ZnFe_2O_4+2CaO\rightarrow Ca_2Fe_2O_5+ZnO$
$3ZnFe_2O_4+C\rightarrow 3ZnO+2Fe_3O_4+CO(g)$
$ZnFe_2O_4+2CaO+C\rightarrow Zn+Ca_2Fe_2O_5+CO(g)$
$Fe_{1-x}O+ZnO\rightarrow Fe_{0.85-x}Zn_xO$
$3Fe_2O_3+C\rightarrow 2Fe_3O_4+CO(g)$
$ZnO+C\rightarrow Zn(g)+CO(g)$
$Fe_{0.85-x}Zn_xO+CaO\rightarrow FeO+Ca_2Fe_2O_5+ZnO$

At α=0.45, the diffraction peaks of FeO are clearly visible, and the diffraction peaks of $ZnFe_2O_4$ disappear. Meanwhile, the clear diffraction peaks of Fe appear, indicating that part of the FeO has been converted to metallic state, and the phases of the reduced sample mainly consist of $Ca_2Fe_2O_5$, FeO, Fe, C and CaO. In consequence, the main reactions in the intermediate stage are shown as below.

$Fe_3O_4+C\rightarrow 3FeO+CO(g)$
$FeO+C\rightarrow Fe+CO(g)$
$ZnO+C\rightarrow Zn+CO(g)$
$Zn(s)\rightarrow Zn(g)$
$Ca_2Fe_2O_5+3C\rightarrow 2CaO+2Fe+3CO(g)$
$Fe_{0.85-x}Zn_xO+CaO\rightarrow FeO+Ca_2Fe_2O_5+ZnO$

With the completion of calcified carbonthermal reduction at α=1.0, the intensity of the diffraction peaks of metallic iron increases while that of FeO decreases, and the diffraction peaks of Fe_3C appear while those of carbon and $Ca_2Fe_2O_5$ disappear. At this moment, the phases of reduced sample are composed of Fe, FeO, Fe_3C and CaO. Thus, the following is a summary of the main reactions at the final stage.

$C+CO_2(g)\rightarrow 2CO(g)$
$FeO+CO(g)\rightarrow Fe+CO_2(g)$
$Ca_2Fe_2O_5+3CO(g)\rightarrow 2CaO+2Fe+3CO_2(g)$
$Fe+3C\rightarrow Fe_3C$

The calcified carbothermal reduction reaction of EAFD at the initial stage, the main reactions include the direct reduction reaction of $ZnFe_2O_4$ with carbon to produce Fe_3O_4 and ZnO, the calcified reaction of $ZnFe_2O_4$ with CaO to $Ca_2Fe_2O_5$ and ZnO, the reduction reaction of ZnO to Zn, and the reduction reaction of Fe_2O_3 to Fe_3O_4. At this time, these reactions are mainly solid-solid reactions, the reaction rate is slow and the average activation energy is high. The diffusion of reactant is dominant in the reaction. With the increase of temperature, the diffusion of carbon is improved and the activation energy decreases and the reaction rate increases. The formation of $Ca_2Fe_2O_5$ shows that CaO can destroy the structure of $ZnFe_2O_4$, which facilitates the reduction and release of zinc, and thereby improves the dezincification ratio of the charge.

The activation energy increases from 261.92 to 381.68 $kJ\cdot mol^{-1}$ with the conversion in the range of 0.3 to 0.45, which is mainly controlled by the interfacial chemical reaction mechanism. Compared to iron oxide, the reduction of $Fe_{0.85-x}Zn_xO$ requires a higher activation energy. In addition, the diffusion of graphitic carbon may be partially hindered by the $Ca_2Fe_2O_5$ formed during the reaction of CaO and $ZnFe_2O_4$ (or $Fe_{0.85-x}Zn_xO$), which coats the unreacted layer. As the reaction proceeds, it is mainly the reduction of Fe_3O_4 and ZnO, and the activation energy does not increase significantly. At a conversion of 0.45, most of the iron oxides have been reduced to FeO.

At the final stage of the reaction (α=0.45-1.0), the intensity of the FeO diffraction peak decreases and that of the Fe diffraction peak increases. Since the reduced metallic Fe can play a catalytic role in the gasification of carbon (Boudouard reaction), the Boudouard reaction is accelerated with increasing temperature [29]. It is well known that the diffusion of CO is easier than that of solid graphitic carbon, i.e., the gaseous reducing agent CO diffuses more easily from the product layers to the unreacted layers, which may lead to an increase in the active sites at the reaction interface. Due to the dominance of the control mechanism of the chemical reaction at the interface, the activation energy starts to decrease after α=0.45. As the reactant concentration continues to decrease in the final phase, the reaction rate also continues to decrease.

CONCLUSIONS

(1) The roasting temperature and carbon ratio are the most important factors affecting the phase transformation and dezincification ratio of EAFD. When the roasting temperature is below 1,000 °C and the carbon ratio n_c/n_o is less than 0.6, zinc ferrite is reduced to a solid solution called intermediate $Fe_{0.85-x}Zn_xO$, which affects the volatilization ratio of Zn. Zinc-iron separation can be improved under low carbon conditions by adding CaO to decompose the zinc ferrite phase and produce the intermediate $Ca_2Fe_2O_5$. The pathway of zinc-iron separation from EAFD is as follows: $ZnFe_2O_4+CaO\rightarrow Ca_2Fe_2O_5+ZnO\rightarrow Ca_2Fe_2O_5+Zn(g)\rightarrow CaO+Fe$; $Fe_{0.85-x}Zn_xO+CaO\rightarrow FeO+Ca_2Fe_2O_5+ZnO\rightarrow CaO+Fe+Zn(g)$. At an n_c/n_o value of 0.4-

1.2 and a roasting temperature of 1,000-1,100 °C, the addition of CaO can promote the reduction and volatilization of zinc, and the amount of calcium oxide added has a small effect on the dezincification ratio.

(2) The calcified carbothermic reduction process of EAFD can be divided into three different stages: α=0-0.3, α=0.3-0.45, and α=0.45-1.0. The average activation energies of the three stages are 305.01, 315.67, and 288.22 kJ·mol^{-1}, respectively. The addition of CaO can obviously decrease the average activation energy of each stage and shorten the intermediate stage of the reaction.

(3) In the first stage (α=0-0.3), the one-dimensional diffusion equation of ($G(\alpha)=\alpha^2$) is considered as a mechanism function. For medium stage (α=0.3-0.45), the chemical reaction equation of $G(\alpha)=1-(1-\alpha)^4$ proves to be more appropriate. The chemical reaction mechanism equation of $G(\alpha)=(1-\alpha)^{-2}$ shows the best fit for the final stage (α=0.45-1.0).

ACKNOWLEDGEMENTS

This research was financially supported by the Open Foundation of State Key Laboratory of Mineral Processing (BGRIMM-KJSKL-2022-12) and the Ph.D. start-up fund of Jiangsu University of Science and Technology (120140004) in China.

CONFLICT OF INTEREST STATEMENT

We declare that we have no financial and personal relationships with other people or organizations that can inappropriately influence our work, there is no professional or other personal interest of any nature or kind in any product.

REFERENCES

1. World Steel Association: https://worldsteel.org.
2. D. Z. Wang, D. Q. Zhu, J. Pan, Z. Q. Guo, H. Y. Tian and Y. X. Xue, *J. Iron Steel Res. Int.*, **2**, 1 (2022).
3. H. Berber, K. Tamm, M. Leinus, R. Kuusik, K. Tonsuaadu, P. Paaver and M. Uibu, *Waste. Manag. Res.*, **38**, 2 (2019).
4. P. J. W. K. D. Buzin, N. C. Heck and A. C. F. Vilela, *J. Mater. Res. Technol.*, **6**, 2 (2017).
5. C. Wang, Y. F. Guo, S. Wang, F. Chen, Y. J. Tan, F. Q. Zheng and L. Z. Yang, *Int. J. Min. Met. Mater.*, **27**, 26 (2020).
6. X. Cao, Z. G. Wen, X. L. Zhao, Y. H. Wang and H. R. Zhang, *Sci. Total Environ.*, **717**, 137114 (2020).
7. D. Z. Wang, D. Q. Zhu, J. Pan, Z. Q. Guo, C. C. Yang, X. Wang and T. Dong, *JOM*, **74**, 2 (2022).
8. J. Q. Song, C. Peng, Y. J. Liang, D. K. Zhang, Z. Lin, Y. Liao and G. J. Wang, *Hydrometallurgy*, **202**, 105599 (2021).
9. A. H. Mohammad, A. N. Jomana, A. O. Awni, A. H. Israa, A. J. Huda, A. Z. Mais and A. A Shaima, *J. Environ. Chem. Eng.*, **7**, 1 (2018).
10. X. L. Lin, Z. W. Peng, J. X. Yan, Z. Z. Li, J. Y. Hwang, Y. B. Zhang, G. H. Li and T. Jiang, *J. Clean. Prod.*, **149**, 1079 (2017).
11. B. S. Kim, J. M. Yoo, J. T. Park and J. C. Lee, *Mater. Trans.*, **47**, 9 (2006).
12. W. Lv, M. Gan, X. H. Fan, Z. Y. Ji and X. L. Chen, *J. Mater. Res. Technol.*, **8**, 6 (2019).
13. T. Guo, X. J. Hu, H. Matsuura, F. Tsukihashi and G. Z. Zhou, *ISIJ Int.*, **50**, 8 (2010).
14. M. H. Morcali, O. Yucel, A. Aydin and B. Derin, *J. Min. Metall. B*, **48**, 2 (2012).
15. Y. X. Zheng, J. Ning, W. Liu, P. J. Hu, J. F. Lu and J. Pang, *Int. J. Min. Met. Mater.*, **28**, 358 (2021).
16. S. Thomas, K. Bart, V. A. Karel and B. Bart, *J. Clean. Prod.*, **65**, 152 (2014).
17. N. Tzouganatos, R. Matter, C. Wieckert, J. Antrekowitscn, M. Gamroth and A. Steinfeld, *Jom-Us*, **65**, 12 (2013).
18. O. Mamdouh and F. Timo, *Sep. Purif. Technol.*, **210**, 867 (2018).
19. C. F. Romchat, I. Yosuke, U. Naoyoshi, I. Satoshi and N. Tetsuya, *Int. J. Min. Met. Mater.*, **22**, 8 (2015).
20. I. Satoshi, T. AKira, M. Y. Kazuyo, N. Kenichi and N. Tetsuya, *ISIJ Int.*, **48**, 10 (2008).
21. C. F. Romchat, M. Katsuya, M. Takahiro and N. Tetsuya, *Hydrometallurgy*, **159**, 120 (2016).
22. M. Takahiro, C. F. Romchat, M. Katsuya and N. Tetsuya, *J. Hazard. Mater.*, **302**, 1 (2016).
23. H. E. Kissinger, *Anal. Chem.*, **29**, 11 (1957).
24. T. Ozawa, *Thermochim. Acta*, **203**, 159 (1992).
25. J. H. Flynn, *Thermochim. Acta*, **203**, 519 (1992).
26. A. W. Coats and J. P. Redfern, *Nature*, **201**, 4914 (1964).
27. R. Z. Hu and Q. Z. Shi, *Thermal analysis dynamics*, Science Press. Publications, Beijing (2008).
28. G. Iwase and K. Okumura, *ISIJ Int.*, **61**, 10 (2021).
29. Y. Z. Liu, X. M. Lu, Z. X. You and X. W. Lu, *Powder Technol.*, **362**, C (2020).